09

Modification of the electronic properties of the $B_{12}SiO_{20}$ crystal by doping it with Fe and Mo

© A.V. Iliinskiy[1], R.A. Castro[2], A.A. Kononov[2], L.A. Nabiullina[3], E.B. Shadrin[1,¶]

[1] Ioffe Institute,
St. Petersburg, Russia
[2] Herzen State Pedagogical University of Russia,
St. Petersburg, Russia
[3] Fire and Rescue College and Rescue Training Center,
St. Petersburg, Russia

¶ E-mail: shadr.solid@mail.ioffe.ru

Received November 29, 2025
Revised November 29, 2025
Accepted January 17, 2026

A comparative analysis of the electronic properties of BSO:Fe and BSO:Mo crystals was performed. It was shown that doping with both impurities is accompanied by two competing processes in these crystals, one of which suppresses dark conductivity, while the other acts in the opposite direction. It was established that the process suppressing dark conductivity is a consequence of the compression of the crystal cells surrounding the cell containing the impurity ion. At the same time, the process that narrows the band gap and, consequently, increases dark conductivity is caused by the effect of the isoelectronic impurity potential on the crystal's energetics, which leads to the lifting of the conduction band degeneracy at the Γ-point of the Brillouin zone. Moreover, the ratio of the contributions of both processes to the modification of the electron-optical properties differs for BSO:Fe and BSO:Mo, determined by the ratio of the ionic radii of the substituting and replaced ions.

Keywords: sillenite crystals, doping, dielectric spectra, charge transfer, Maxwell relaxation time.

DOI: 10.61011/PSS.2026.01.63255.337-25

1. Introduction

Currently, crystals of the sillenite group are widely used in optical technologies and are used, for example, for non-contact deformation control and flaw detection of load-bearing structures in the automotive industry, mechanical engineering and aircraft industry [1]. However, these crystals are also interesting from a fundamental point of view. They have a photorefractive effect: a unique combination of optical and electrical properties that allows real-time recording and processing of optical images, including holographic ones, as well as effective modulation of light fluxes. In addition, an interesting phenomenon has been discovered in BSO crystals: space charge stratification, which occurs during the shielding of an external electric field by a crystal [2]. The phenomenon of stratification is based on such a unique phenomenon as the generation of spatial recharge waves of traps, theoretically predicted by R. Souris, R. Kazarinov, and B. Fuchs in 1972 [3]. Spatial recharge waves in BSO crystals were studied in detail in Refs. [4–6]. To date, extensive material has been accumulated on the optical, electro-optical and photoconductive properties of sillenites, including in sillenites doped with various impurities.

In the course of these studies, it has been shown that the optical and photoelectric properties of crystals with a sillenite structure are largely determined by defective centers whose energy levels are located in the band gap [7]. The reason for the appearance of such defective centers in Ref. [8] is associated with background impurities, as well as structural or stoichiometric disturbances that occur in sillenite crystals as a result of annealing in air or in vacuum, which leads to the appearance of „shoulder" absorption in the range of $\lambda = (380-500)$ nm. Currently, there is an opinion that the contribution to the formation of the „shoulder" is largely due to the fundamental properties of sillenites, which are not related to the formation of any defects. Namely, we are talking about the effect of a high concentration of lone electron pairs in a BSO crystal due to the hybridization of oxygen ions present in each crystal cell in the amount of 20 units. At the same time, the contribution to the formation of the „arm" in the absorption spectrum is associated with the donor properties of stoichiometric defects [9], is also the case.

It should be emphasized that, despite the achievements in the field of studying the physical properties of doped sillenites, achievements in the field of dielectric spectroscopy of compounds of the sillenite group are limited: the nature and parameters of electronic relaxers have not been studied sufficiently, and all existing model representations in this field are limited. At the same time, the methods of dielectric spectroscopy with the current level of development of its element base are able to provide an extensive package of new fundamental information in many areas of solid state physics, including the physics of sillenites.

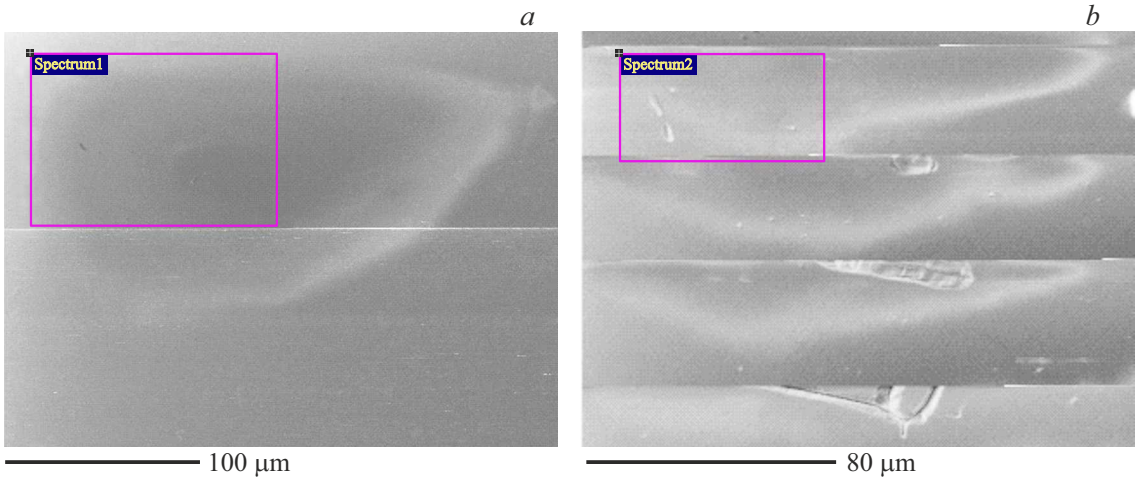

Figure 1. Surface scans of undoped (a) and molybdenum-doped (b) crystals of $B_{12}SiO_{20}$.

In this regard, the purpose of this work was to identify by dielectric spectroscopy the features of charge transfer processes in sillenite crystals doped with an admixture of iron and molybdenum, as well as a comparative analysis of the effect of such doping on the electronic properties of sillenites.

2. Experimental procedure

The object of the study was samples of bismuth silicate $Bi_{12}SiO_{20}$ grown by the Chokhralsky method and doped with iron (Fe) and molybdenum (Mo) ions. The samples were made in the form of discs with a diameter of 20.0 mm and a thickness of 1.0 mm.

The structural features of the samples were studied by scanning electron microscopy (SEM), namely, using a Carl Zeiss EVO 40 scanning electron microscope. The high resolution of the device made it possible to use both the direct electron irradiation mode and the reverse electron scattering mode in surface studies. Metal diaphragms that cut off stray streams of scattered electrons made it possible to obtain high-quality images of the dielectric surface in low vacuum conditions. In addition, this microscope allowed for the analysis of electron diffraction patterns, chemical microanalysis, topography of the distribution of elements over the surface, as well as variations in the distribution of chemical phase composition over the surface of samples.

Arbitrary points on the surface were selected to determine the topography of the chemical composition of the sillenite crystal samples (Figures 1, 2). The appearance of molybdenum atoms on the surface of the samples is detected on the atomic spectra (Figures 3, 4). Tables 1, 2 provide data on the percentage of chemical elements in samples of sillenite crystals before and after doping.

Measurements of the dielectric spectra (DS) of the samples were carried out on a „Concept-41“ spectrometer (CUC of Dielectric Spectroscopy of the Research Institute

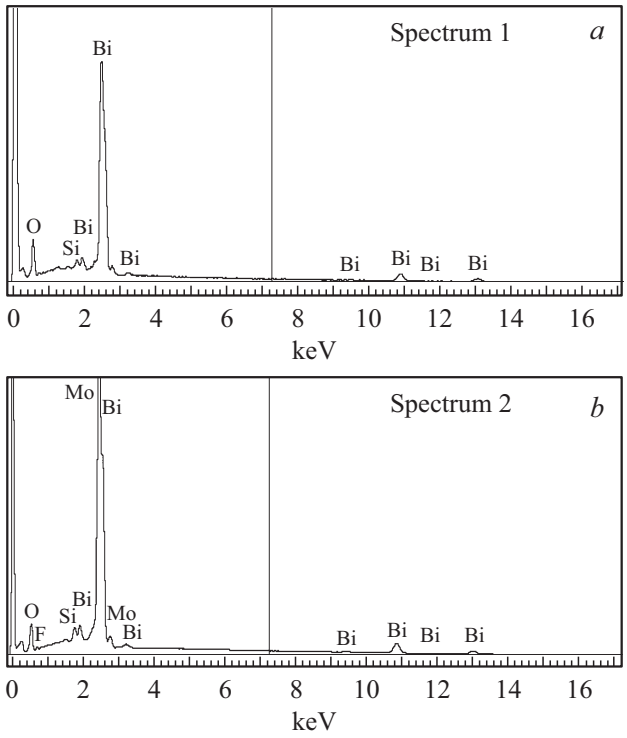

Figure 2. SEM spectra of undoped (a) and molybdenum-doped (b) sillenite crystals

of Physics). The measuring system consisted of an ANB frequency impedance analyzer, a cryostat with a measuring cell, a temperature control system, an automatic data acquisition system, and a Dewar vessel with a nitrogen gas supply system. The impedance analyzer included an alternating voltage generator applied to the sample and a current analyzer that measured both the numerical value of the amplitude of the sinusoidal current and the phase shift of current fluctuations relative to generator voltage fluctuations. In this case, an alternating voltage with an amplitude of $U(t) = 1$ V

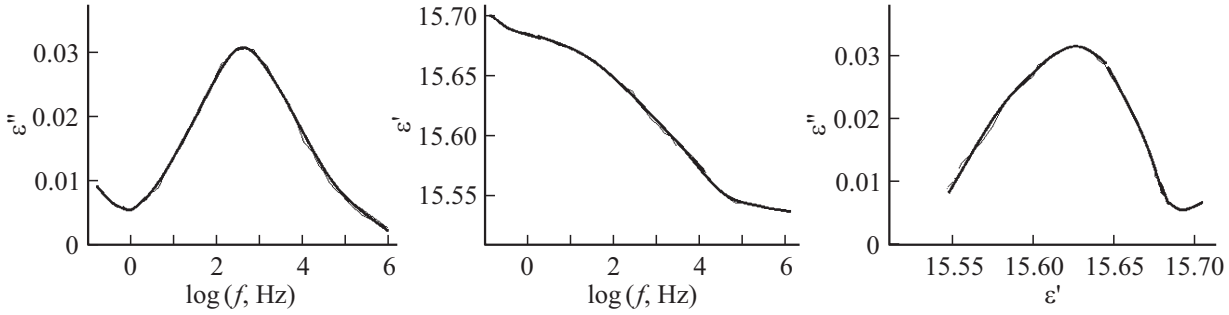

Figure 3. Frequency dependences of the imaginary $\varepsilon''(f)$ and real $\varepsilon'(f)$ components of the complex permittivity ε^* and the Cole-Cole diagram $\varepsilon''(\varepsilon')$ for the crystal BSO : Fe.

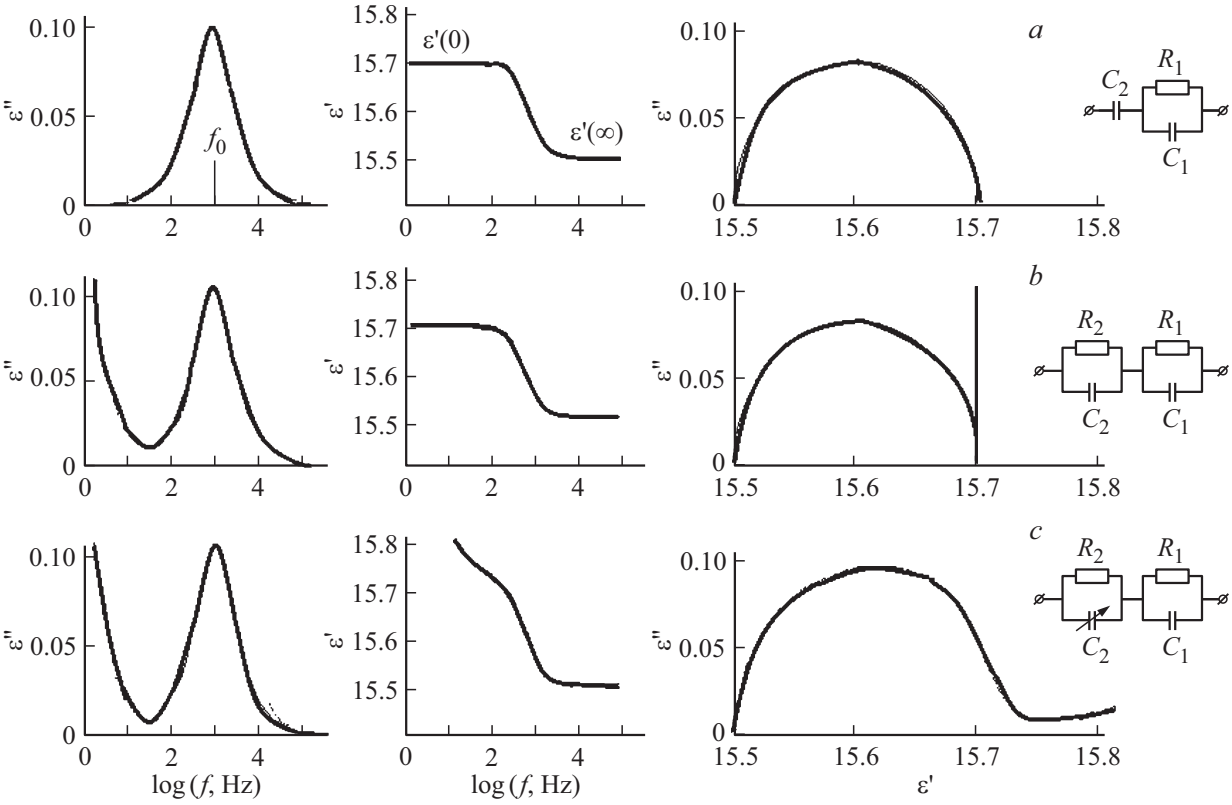

Figure 4. The results of DS calculations according to successively more complicated equivalent schemes: the frequency dependences of the imaginary $\varepsilon''(f)$ and real $\varepsilon'(f)$ parts of the complex permittivity ε^*, as well as the Cole-Cole diagrams $\varepsilon''(\varepsilon')$. $R_1 = 5 \cdot 10^3\,\Omega$, $R_2 = 1 \cdot 10^{12}\,\Omega$, $C_1 = 1200\,\text{pF}$, $C_2 = 15.7\,\text{pF}$. For Figure 4, *c*: $C_2(f) = 15.7 + 1 \cdot f^{-0.5}\,\text{pF}$.

was applied to the sample from the master generator, and measurements of the parameters of the current $I(t)$ flowing through the sample were carried out. The phase difference between current and voltage fluctuations was used to calculate the spectra of the complex impedance of the sample, which were used to determine the values of the real and imaginary components of the complex permittivity [10,11].

3. Experimental results and their analysis

To identify the features of charge transfer processes, the study of DS (frequency dependences of complex dielectric constant) in doped samples of sillenite crystals $Bi_{12}SiO_{20}$: Fe,Mo (BSO : Fe,Mo) was carried out in the frequency range of $f = 10^{-2} \cdot 10^4$ Hz.

Figure 3 shows the frequency dependences of the imaginary $\varepsilon''(f)$ and real $\varepsilon''(f)$ components of the complex permittivity ε^* and, in addition, the Cole-Cole diagram $\varepsilon''(\varepsilon')$ of the BSO : Fe sample.

The frequency dependence function $\varepsilon''(f)$ demonstrates a wide maximum at the frequency of 10^3 Hz, its frequency position is in the middle of the step of the real part $\varepsilon'(f)$, and the Cole-Cole diagram $\varepsilon''(\varepsilon')$ is a strongly distorted semicircle. In addition to these elements of the dielectric spectra, additional spectral features were observed at low

Table 1. Elemental composition of undoped samples of sillenite crystals $Bi_{12}SiO_{20}$

Element	Relative concentration	Relative signal intensity electronic flux	Weight %	Relative error (%)	Atomic %
O	0.70	0.7127	56.87	1.08	92.59
Si	0.03	0.6382	2.54	0.25	2.35
Bi	0.54	0.7632	40.59	1.08	5.06
Results			100		

Table 2. Elemental composition of $Bi_{12}SiO_{20}$sillenite crystal samples doped with molybdenum admixture

Element	Relative concentration	Relative signal intensity electronic flux	Weight %	Relative error (%)	Atomic %
O	8.85	0.6398	41.98	0.34	76.53
F	0.41	0.1460	8.62	0.42	13.04
Si	0.74	0.6402	3.53	0.06	3.66
Mo	0.28	0.8209	1.03	0.22	0.51
Bi	11.59	0.7851	44.83	0.35	6.26
Results			100		

frequencies in the form of a monotonous rise $\varepsilon''(f)$ and $\varepsilon'(f)$ in the direction of zero frequencies and, as a result, a continuous increase in the numerical values of the function $\varepsilon''(\varepsilon')$ on the Cole-Cole diagram for large values ε' (namely, for „zero“ frequencies).

The results obtained are described in the first approximation within the framework of a single-circuit model, represented by the insert in Figure 4, *a*.

Here R_1 is the resistance of the crystal sample, C_1 is its capacitance, and C_2 is the capacitance of the thin electrode layer of the crystal plate. The reference points in Figure 4 correspond to: $\varepsilon'(0) = C_2/C_0, C_1 \cdot C_2/[(C_1 + C_2)C_0]$, $f_0 = 1/(2\pi R_1 C_1)$, where C_0 is the capacitance of the sample-free cell of the dielectric spectrometer.

According to this model, the frequency position of the maximum of the imaginary part of the complex permittivity $f_0 = 1/(2\pi R_1 C_1,) = 1/(2\pi\tau_M)$ is determined by the Maxwell relaxation time $\tau_M = \varepsilon\varepsilon_0/\sigma$, where σ is the specific conductivity of the crystal. For BSO : Fe, the frequency $f_0 = 10^3$ Hz corresponds to $\tau_M = 1.6 \cdot 10^{-4}$ s and $\sigma = 10^{-6}\,\Omega^{-1}\mathrm{m}^{-1}$. Thus, the Fe impurity makes the sillenite sample not as highly resistant as undoped samples or samples doped with other impurities (Mo, Al and etc.). It should be also noted that in the single-circuit model electrical circuit, the step height $\varepsilon'(f)$ and the maximum height $\varepsilon''(f)$ are significantly higher than the experimental values, i. e., the experimental semicircle is strongly „flattened“. It should be noted that the simplest model electrical circuit of the sample does not describe the low-frequency features of DS. It turned out that in order to describe DS that include these features, an additional resistance R_2 should be introduced into the equivalent circuit, taking into account the possibility of through current flowing between the crystal and the metal electrode (see the diagram in the box Figure 4, *b*). Figure 4, *b* shows the result of the DS calculation for such an upgraded scheme.

Here, a corresponding nonzero signal already appears in the low-frequency region of the spectrum $\varepsilon''(f)$, and an almost vertical straight line for the zero frequency appears on the diagram $\varepsilon''(\varepsilon')$. This calculation better corresponds to the experiment, but it does not explain the increase of $\varepsilon'(f)$ at $f \to 0$ and the significant deviation of $\varepsilon''(\varepsilon')$ from the vertical at values ε' greater than C_2/C_0. To solve this problem, it is customary in the literature to include a Warburg element in an equivalent circuit, the use of which means abandoning linear equivalent circuits. In our case, it makes sense to introduce a frequency dependence of the capacitance in the form of $C_2(f) = A + B \cdot f^{-0.5}$. Figure 4, *c* shows the calculation result according to the electrical circuit shown in insert 4, *c*, which is performed taking into account the dependence of the electrical capacity $C_2(f)$ on frequency.

Turning to the discussion of the results, we note first of all that the experimentally measured features of DS are much broader than those obtained as a result of calculations using the proposed equivalent schemes. This is clearly evident in the „flattened“ semicircle shape on the Cole-Cole diagram. A natural explanation for this fact is the

statement that there is more than one type of relaxers in the crystal, but there is a whole set of relaxers distributed according to numerical values of relaxation times. A real sample of a sillenite crystal is characterized by a set of Maxwellian relaxation time values distributed over a wide time range, which is associated with a spread of crystal conductivity values $\sigma = e\mu n$, where e is the electron charge, μ is its drift mobility, n is the concentration of equilibrium electrons. A consequence of this fact is the broadening of the experimental features of the DS in comparison with the calculated ones, which is due to the spread of numerical values of electron mobility determined by their drift under conditions of capture by traps of various types.

The presence of relatively high (compared to non-doped crystals) conductivity of iron-doped sillenite crystals indicates a narrowing of the band gap of the BSO crystal as a result of doping. This is due to the peculiarities of the incorporation of the Fe atom into the crystal lattice of BSO. A detailed scheme of such embedding is given in Ref. [12]. The iron ion replaces the Si^{4+} ion during doping and, like Si^{4+}, has four σ-bonds with oxygen ions. These bonds are formed as a result of hybridization, the structure of which is described in this paper below in the section devoted to the description of the physical properties of the crystal BSO : Fe.

We also note that the introduction of additional resistance R_2 into an equivalent circuit in calculations leads to additional dielectric losses at low frequencies due to the following reasons. Namely, through the resistors R_1 and R_2, a through-drift electron current flows at $f \to 0$, and there is no bias current through the series capacitances C_1 and C_2 in this case. At the same time, the numerical value of the phase difference δ between fluctuations in current and applied voltage (the angle δ of dielectric losses) is close to $\pi/2$ ($\delta \sim 90^\circ$). This value of angle δ corresponds to an almost vertical straight line on the Cole-Cole diagram.

However, as already noted, the experimental graph of the function $\varepsilon''(\varepsilon')$ does not contain a vertical line. This fact requires additional complication of the equivalent electrical circuit of the sample. This complication was carried out in this paper by including in the calculations the ideology of capacity growth C_2 as the frequency decreases. This variant of complicating the circuit is justified from the point of view of the physics of the processes occurring in BSO by the well-known fact that when an external constant electric field is applied to a crystal in the near-electrode region of the crystal, a positive volume charge is formed from the negative electrode, due to the drift of free electrons towards the positive electrode. The spatial extent of the volume charge region decreases over time, and the volume charge density increases. Such a change in the spatial charge area corresponds to an increase in the near-electrode electrical capacity of the system. Obviously, at high frequencies, the oscillation period of which is less than τ_M, such a layer does not have time to form, whereas at low frequencies it turns out to be less wide and with a higher volume charge density, the lower the frequency of the applied field. Thus, replacing the constant value C_2 with a frequency-varying capacitance of the type $C_2(f) = A + B \cdot (f)^{-0.5}$ allows aligning the calculation results with the measurement data.

Turning to the results of the study of doped BSO crystals, we note that the case of doping of sillenites with Fe atoms studied in this paper is of particular interest [13], since it agrees with the data provided in Ref. [12] and confirms the fact that trivalent ions of Fe^{3+} occupy tetra-coordinated positions, replacing Si^{4+} ions, which also coincides with the conclusions in Ref. [14]. In this case, all oxygen ions surrounding the Si^{4+} ion in the crystal cell are also tetra-coordinated [12].

During the formation of the standard σ bond between silicon and oxygen, the ion Si^{4+} is in a state of $3s^2(1)3p^2(3)$-hybridization (the number of orbitals involved in hybridization is indicated in parentheses, the upper indices show the number of electrons on them), and the oxygen ion is either in the state of $2s^2(1)2p_x^1(1)2p_y^1(1)3s^0(1)$-hybridization, or in the state of $2p^4(3)3s^0$ (1)-hybridization (recall that, according to the theory [14], the number of hybrid orbitals coincides with the number of atomic orbitals involved in the formation of hybrid orbitals). In both of these states, the four hybrid orbitals of the oxygen ion contain one electron each and form four standard σ-bonds: one with Si^{4+}, the other three with Bi^{3+}.

It should be noted that, along with the described variant of oxygen ion hybridization, the undoped BSO crystal contains oxygen ions hybridized in a different form. Namely, there are oxygen ions that, while still forming four hybrid orbitals, are in a state of $2s^2(1)2p_x^1(1)2p_y^1(1)2p_z^2(1)$-hybridization. In this variant of hybridization, two of the four hybrid orbitals contain one electron each, and the other two contain a pair of electrons with oppositely directed spins. Since the Si^{4+} ion forms standard σ-bonds with oxygen ions, taking one electron each from it, the two orbitals of the tetra-coordinated oxygen ion containing electron pairs must form donor-acceptor (coordination) bonds with the corresponding vacant orbitals of the two Bi^{3+} ions. Bi^{3+} ions, being hepta-coordinated, form three standard σ-bonds with O ions, as well as four donor-acceptor bonds with these ions. It follows from the above that, in order to create a closed electronic configuration, it is necessary to have three coordinated oxygen ions in the sillenite lattice in the state of $2p_x^1(1)2p_y^1(1)2p_z^2(1)2s^2(1)$-hybridization, which, according to X-ray diffraction analysis, are present in the sillenite lattice.

By calling such a structure „three-coordinated“, we mean that three hybrid ion orbitals O forms standard σ-bonds with Bi^{3+} ions, whereas on the fourth, a free lone electron pair is localized, which does not participate in the formation of a chemical bond. X-ray data from Ref. [15] confirm this assumption, indicating the presence of valence bonds of a three-valence oxygen ion with a bismuth ion that do not lie in the same plane, as should be the case with the existence of an unshared electron pair in the fourth hybrid orbital. It should be noted that there are no two-coordinated oxygen ions in the sillenite lattice.

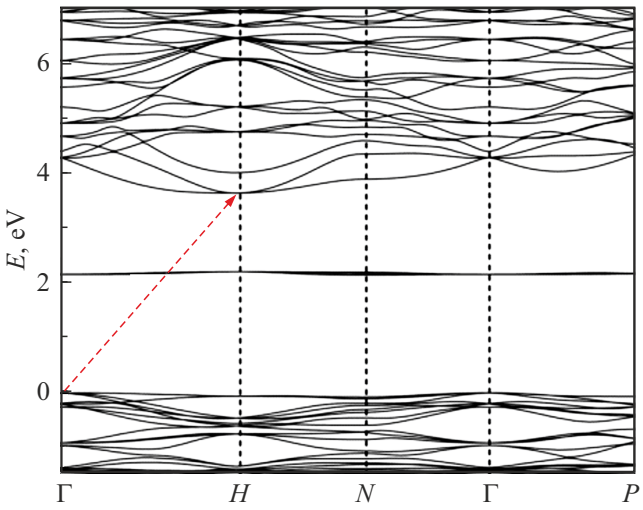

Figure 5. The structure of the energy bands of the crystal $Bi_{12}SiO_{20}$.

In the Fe-doped BSO crystal, the trivalent silicon ion is replaced by a trivalent iron ion. The iron ion can be in the state of Fe^{3+} with $3d^1(1)4s^2(1)4p_x^0$ (2) hybridization or in the state with Fe^{3+} hybridization $3d_{xy}^1(1)4s^2(1)4p_x^0(1)4d_{xy}^0(1)$. The latter option cannot be ruled out for reasons of generality, although it is unlikely. In any case, the three-valence, four-coordinated iron ion Fe^{3+} has one free orbital capable of creating a donor-acceptor (coordination) bond by accepting an electron pair from the hybrid orbital of the neighboring four-coordinated oxygen ion in the state of $2s^2(1)2p_x^1(1)2p_z^2(1)2p_y^1(1)$-hybridization. It is obvious that this oxygen ion is in a state with an uneven distribution of electron density over its hybrid orbitals (the theory allows for such a distribution variant [16]). Here, there are six electrons per four orbitals, that is, two electron pairs are fixed in two orbitals. One of them is given to the free orbit of the tetra-coordinated Fe^{3+} (see below in Figure 8, *a*), and the other is given to the free orbit of the hepta-coordinated Bi^{3+}.

The orbitals of the Fe^{3+} ion, having one electron each, receive one electron from oxygen ions in the state of $2s^2(1)2p_x^1(1)2p_y^1(1)3_s^0(1)$-hybridization. This variant of oxygen ion hybridization means that the orbitals of the Bi^{3+} ion, with which these oxygen ions form standard σ-bonds, also delegate one electron to these σ-bonds.

It follows from the analysis that the iron ion introduced into the BSO lattice during doping and replacing the four-coordinated silicon ion forms four hybrid atomic orbitals similarly to the silicon ion it replaces. This fact indicates that the iron ion is an isoelectronic ion relative to the silicon ion in $Bi_{12}SiO_{20}$. This, in turn, means that the theory of electron band anti-intersection can be applied to explain the narrowing of the band gap of a BSO crystal when it is doped with an isoelectronic admixture of iron, since the necessary degeneracy of the electronic bands takes place at the Γ-point of the Brillouin band, shown in Figure 5 [17].

According to this theory, under the influence of the potential of an isoelectronic impurity, the degeneracy of the conduction band is removed. The removal of the degeneracy of the conduction band is accompanied by its splitting into several components, of which at least one decreases in energy relative to its non-split position, which leads to a narrowing of the band gap E_g [18]. The degree of narrowing turns out to be proportional to the impurity concentration, shifting the position of the edge of fundamental absorption to the long-wavelength side [12].

At the same time, in the case of BSO:Fe, there is an opposite factor that manifests itself only at low (up to 3 %) concentrations of the doping impurity Fe. Namely, by comparing the ionic radii of a silicon ion and an iron ion replacing it, we are convinced that the iron ion has a radius (0.052 nm) slightly larger than the silicon ion it replaces (0.039 nm). For information, we present data from Ref. [19]: Al^{4+} 0.035 nm (0.35 Å), Si^{4+} 0.039 nm (0.39 Å), Fe^{4+} 0.052 nm (0.52 Å), Mo^{4+} 0.089 nm (0.89 Å). It follows from this that the iron ion during doping pushes apart, albeit slightly, the surrounding ions of the crystal cell, inevitably subjecting to compression those crystal cells that surround the cell with the Fe^{3+} ion, but at the same time do not contain the Fe^{3+} ion. And since the compression voltage causes a certain expansion of the band gap [20], the edge of the fundamental absorption of the BSO crystal during its Fe doping is slightly shifted to the short-wavelength region of the spectrum. It is important that the concentration of the doping impurity in this case is small (3,%), so that the effect of the disturbing effect of the impurity potential is vanishingly small, leading to splitting of the conduction band at Γ, which narrows E_g when removing the degeneracy of the band. The experiment confirms this conclusion [21]. Let's pay attention to the fact that, according to [21], in the long-wavelength region of the spectrum, the optical absorption coefficient increases slightly as a result of Fe doping, which indicates a slight influence on the optical absorption spectrum of another factor, namely, the generation factor during doping of oxygen vacancies with donor properties, which slightly increases the extinction coefficient in the „arm" region optical absorption.

Turning to the case of doping a $Bi_{12}SiO_{20}$ crystal with an admixture of molybdenum, we point out that the dielectric spectra (DS) of the BSO:Mo sample look completely different. First of all, we note that the values of the signals for $\varepsilon''(f)$ and $\varepsilon'(f)$ are two orders of magnitude smaller here. Moreover, it is so much smaller that at room temperature it is not possible to register DS in the normal measurement mode ($U = 1$ V). Signal recording is possible only at elevated temperatures ($T \geq 100\,^\circ$C) of the samples (Figure 6).

Figure 6 shows that at a low temperature ($T \sim 100\,^\circ$C), all the features of the DS are located at extremely low frequencies, which are practically not included in the detection range of the dielectric spectrometer. Therefore, in this article, the measurement results are given for the

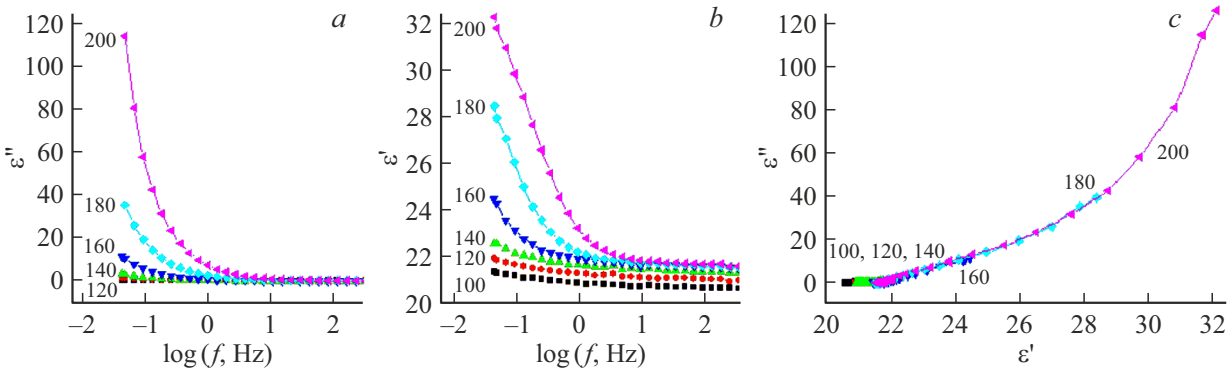

Figure 6. Frequency dependences of the imaginary $\varepsilon''(f)$ and real $\varepsilon'(f)$ parts of the complex permittivity ε^* and the Cole-Cole diagram $\varepsilon''(\varepsilon')$ for a BSO:Mo crystal at temperatures 100–200 °C.

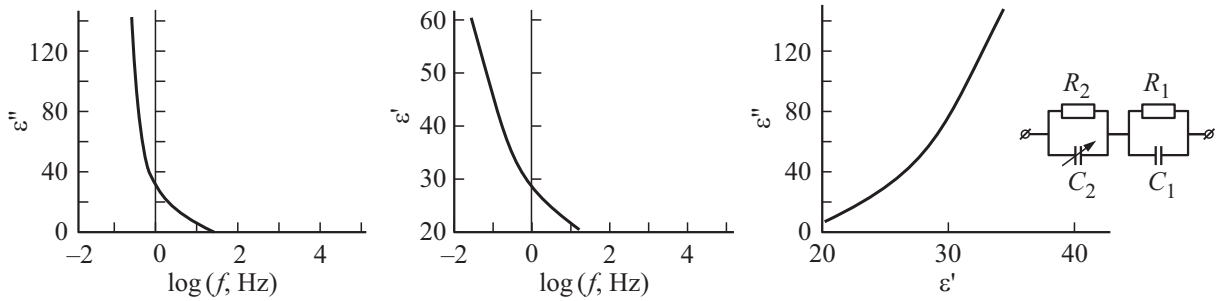

Figure 7. The results of calculations of the frequency dependences of the imaginary $\varepsilon''(f)$ and real $\varepsilon'(f)$ parts of the complex permittivity ε^* and Cole-Cole diagrams $\varepsilon''(\varepsilon')$. Here $R_1 = 10^9\,\Omega$, $R_2 = 1 \cdot 10^{10}\,\Omega$, $C_1 = 55\,\text{pF}$, $C_2 = 32\,\text{pF}$.

temperature range $100 < T \leq 200\,^\circ$C. For this temperature range, the maximum on the graph of the function $\varepsilon''(f)$ and the step on the graph of the function $\varepsilon'(f)$ are only partially included in the available frequency range of measurements. We will specify. that the Cole-Cole diagram shows a strong monotonous increase in the values of the function $\varepsilon''(\varepsilon')$ in the region corresponding to low frequencies (Figure 6). Moreover, the numerical values of the functions $\varepsilon''(f)$ and $\varepsilon'(f)$ increase sharply with increasing crystal temperature, so that in the Cole-Cole diagram $\varepsilon''(\varepsilon')$ each curve corresponding to a higher temperature is a continuation of the previous curves.

The results of calculations of the frequency dependences of the imaginary $\varepsilon''(f)$ and real $\varepsilon'(f)$ parts of the complex permittivity ε^* and Cole-Cole diagrams $\varepsilon''(\varepsilon')$. Here $R_1 = 10^9\,\Omega$,

$$R_2 = 1 \cdot 10^{10}\,\Omega, \quad C_1 = 55\,\text{pF}, \quad C_2 = 32\,\text{pF}.$$

The results obtained for all temperatures used are described in the framework of the model equivalent scheme shown in the box in Figure 7 (this figure shows the calculation results only for the maximum temperature of the sample: $T = 200\,^\circ$C).

According to this model, at zero frequencies (stationary case), a through current flows through the sample, the flow of which is ensured by the presence of R_1 and R_2 resistors on the equivalent circuit. This means that charge is transferred by conduction electrons along a closed circuit at zero frequency, and Joule heat is released, accompanying energy losses during their interaction with phonons. At the same time, the displacement current through the capacitances C_1 and C_2 in such an electrical circuit turns out to be absent, that is, the tangent of the dielectric loss angle at zero frequency in such a simplified circuit increases almost indefinitely ($\text{tg}\,\delta(f) \to 0$ at $f \to 0$), providing a phase difference value δ at $f \to 0$ equal to $\pi/2$. However, this conclusion does not correspond to the experimental results. In this regard, to coordinate the experimental results and the calculation results, a variable capacitance $C_2(f) = A + B \cdot (f)^{-0.5}$ was introduced into an equivalent circuit, which makes it possible to adequately describe the strong monotonous increase in the values of the function $\varepsilon''(\varepsilon')$ in the region corresponding to low frequencies $f(\log(f) < -1)$.

It should be noted that for BSO:Mo, the frequency 10^{-2} Hz corresponds to $\tau_M = 16\,\text{s}$ and $\sigma = 10^{-11}\,\Omega^{-1}\text{m}^{-1}$. This means that, compared with unalloyed BSO samples or BSO samples doped with other impurities (Fe, Co, Mn), the Mo impurity, when introduced into the sillenite sample, leads, for example, like the Al admixture [22] to the expansion of the band gap of the BSO:Mo crystal, which makes it very high-resistance. It should be noted in passing that although this fact is valuable for the practical use of

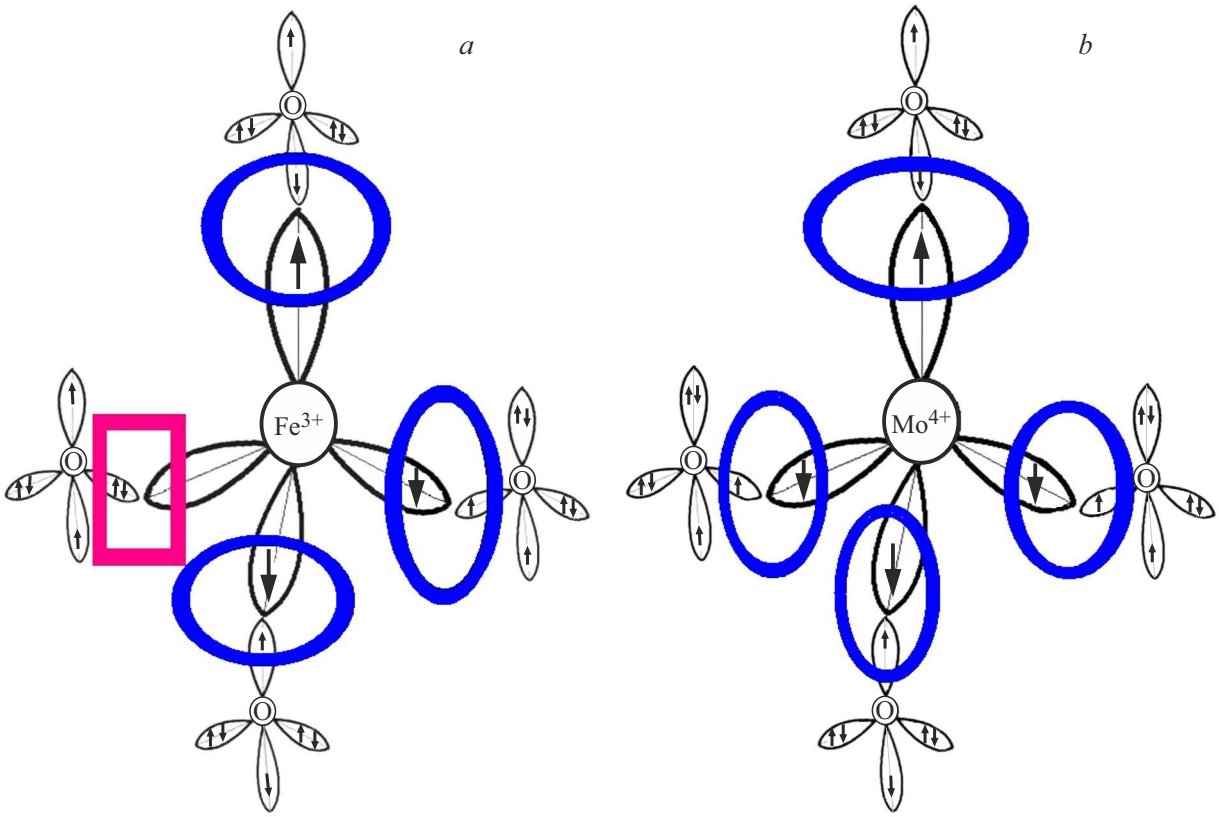

Figure 8. Chemical bonds of the tetra-coordinated trivalent ion Fe^{3+} (a) and the tetra-coordinated tetravalent ion Mo^{4+} (b) introduced into the crystal lattice of BSO when they substituted the base ion Si^{4+}. The figure demonstrates the fact that one of the hybrid molecular orbitals of the Fe^{3+} ion is free of electrons, which leads to the formation of a donor-acceptor chemical bond of this ion with an ion of four coordinated oxygen ions. There is no such connection type for BSO:Mo^{4+}.

sillenites, it greatly complicates the study of charge transfer processes occurring in these crystals.

The experiment shows a monotonous increase in the values of the function $\varepsilon''(f)$ with a decrease in the frequency of the probing electric field, and the dielectric loss angle δ turns out to be significantly smaller $\pi/2$. The consequence of the inconsistency of the calculation results using a simplified equivalent electrical circuit with the experimental data is the need to complicate the equivalent electrical circuit used in the calculations. Such a complication may be, for example, the use, as mentioned above, of the idea of increasing the capacity of C_2 as the frequency of the probing field decreases. Obviously, at $\tau_M = 16\,s$ at high frequencies ($\log(f) \sim 1-5$), the spatial layer does not have time to form, so its width is determined by the length of the electron drift. At the same time, at low frequencies ($\log(f) < -1$), the density of the charged charge increases, and its width decreases with decreasing frequency of the applied probing electric field [23]. Thus, replacing the constant value of the capacitance $C_2 = \text{const}$ with a function $C_2(f)$ corresponding to the frequency dependence of the capacitance type $C_2(f) = A + B/f$ is justified, allowing the calculation results to be consistent with the measurement data.

The absence of a DS signal acceptable for measurements at room temperature is due to the specific properties of the molybdenum atom introduced into the crystal lattice during the synthesis of the sillenite crystal.

Namely, the Mo atom has the initial electronic configuration $Kr[4d^5(5)4f^0(7)5s^1(1)5p^0(3)]$. By replacing the Si^{4+} ion during doping of the BSO crystal, the Mo atom forms, unlike the Fe^{3+} ion, four hybrid molecular orbitals containing one electron each and forming standard σ bonds with oxygen ions. Here, as indicated in the section devoted to the description of BSO:Fe, ion Si^{4+}, before its replacement by ion Mo^{4+}, is in the state of $3s^2(1)3p^2(3)$-hybridization, forming standard σ-bonds with oxygen ions, and oxygen ions are in a state of $2s^2(1)2p^1(1)2p^1(1)3s^0(1)$-hybridization. In these states, the four hybrid orbitals of the oxygen ion contain one electron each and form four standard σ-bonds before doping: one with Si^{4+}, and the rest with the Bi^{3+} ion. During the doping process, four hybrid orbitals of the Mo^{4+} ion are formed according to the following scheme:

$$4d^1_{z2}(1)4d^1_{xy}(1)4d^1_{x2-y2}(1)5s^1(1)$$

and form, like the ion Si^{4+}, four standard σ-bonds with oxygen ions.

Chemical bonds of the tetra-coordinated trivalent ion Fe^{3+} (a) and the tetra-coordinated tetravalent ion Mo^{4+} (b) introduced into the crystal lattice BSO in the process of replacing the base ion Si^{4+}. The figure shows the fact that one of the hybrid molecular orbitals of the Fe^{3+} ion is free of electrons, which leads to the formation of a donor-acceptor chemical bond of this ion with an ion of four coordinated oxygen ions. There is no such connection type for $BSO:Mo^{4+}$.

Figure 8 shows that both the Fe^{3+} ion and the Mo^{4+} ion are isoelectronic with respect to the basic crystal lattice of $Bi_{12}SiO_{20}$, despite the fact that they have different valences. The fact is that the numerical value of valence is determined by the number of electrons given by a given element to a chemical bond, whereas isoelectricity is determined by the coincidence of the number of bonds of the substituting and substituted ions with the crystal lattice, which is not the same thing [24]. The fact of isoelectronicity also makes it possible to use the theory of electron band anti-intersection in the case of BSO:Mo [25] to explain the effects of an doping impurity on the electronic spectrum of a doped crystal.

As mentioned above, according to this theory, when an isoelectronic impurity (IEP) is introduced into a crystal with a sharp discrepancy between its physical parameters (radius, length, and strength of chemical bonds) and the physical parameters of the doped crystal, its band structure changes due to local distortion of the lattice by the impurity. The energy levels corresponding to the impurity resonantly interact with the conduction band, removing its degeneracy at the Γ-point of the Brillouin band. In this case, new hybrid states are formed, which form two subbands with minima at $k = 0$ [26]. As a result, the conduction band is divided into an upper narrow subband E^+, formed by highly localized states, and a lower wider subband E^-, formed by delocalized (extended) states.

As for the reason for the exceptionally strong suppression of the dark conductivity of the BSO:Mo crystal described above, it becomes clearer if we take into account the ratio of the ionic radii of the Mo^{4+} ion and the ion Si^{4+} replaced by it. Namely, the radius Si^{4+} is 0.039 nm, while the radius Mo^{4+} is 0.089 nm [19]. Since these radii differ by half, the Mo^{4+} ion occupies a volume 8 times larger in the BSO crystal cell than the volume occupied before doping by the ion Si^{4+}. According to the literature data [27,28], both the all-round and uniaxial compression of the BSO crystal lead to an expansion of the band gap. This factor suppresses the conductivity of the sillenite crystal, which is confirmed by the experimental results of this work.

The expansion of the energy band gap of BSO crystals during their Mo doping is also confirmed by the literature data [29]. A general optical illumination of the crystal occurs simultaneously with the expansion. The reason here is the same as the reason for suppressing dark conduction. Namely, it has been proven in Ref. [30] that high external pressure not only does not lead to the appearance of oxygen vacancies in $Bi_{12}SiO_{20}$ (BSO), which increase its conductivity, but, on the contrary, suppresses their formation during crystal synthesis under high pressure.

4. Conclusion

In this paper, a comparative analysis of the optoelectronic properties of BSO:Fe and BSO:Mo crystals is performed. It is shown that doping with both impurities is accompanied by two mutually competing processes, one of which suppresses the dark conductivity of crystals, while the other acts in the opposite direction. At the same time, the ratio of the contributions of both processes to the modification of the electro-optical properties of the BSO crystal is sharply different for the cases of Fe and Mo doping and is determined by the ratio of the ionic radii of the substituting and substituted ions. The process that suppresses dark conductivity is a consequence of the compression of the crystal cells surrounding the cell containing the impurity ion. The process that narrows the band gap and, consequently, increases the dark conductivity is caused by the resonant effect of the isoelectronic impurity potential on the crystal energy, which leads to the removal of the degeneracy of the conduction band at the Γ-point of the Brillouin band and causes a narrowing of E_g.

Funding

The study was partially supported by funding from an internal grant from the A.I. Herzen Russian State Pedagogical University: project No.50-VG.

Conflict of interest

The authors declare that they have no conflict of interest.

References

[1] A.A. Kolegov, L.A. Kabanova. V sb.: Fizika tverdogo tela: Sbornik materialov XII Rossijskoj nauchnoj studencheskoj konferencii. TGU, Tomsk (2010). p. 163 (in Russian).
[2] V.N. Astratov, A.V. Ilyinsky, V.A.Kiselyov. FTT **26**, *9*, 2843 (1984) (in Russian).
[3] R.F. Kazarinov, R.A. Suris, B.I. Fuks. FTP **6**, *3*, 572 (1972) (in Russian).
[4] V.V. Bryksin, M.P. Petrov. FTT **42**, *10*, 1809 (2000) (in Russian).
[5] M.P. Petrov, V.V. Bryksin, H. Vogt, F. Rahe, E. Kraetzig. Phys. Rev. B **66**, *8*, 107 (2002).
[6] V.V. Bryksin, P. Kleinert, M.P. Petrov. FTT **46**, *9* 1566 (2004) (in Russian).
[7] A.S. Akrestina. Avtoref. kand. diss. Tomskij politekhnicheskij institut, Tomsk (2014) (in Russian).
[8] A.M. Plesovskikh, S.M. Shandarov, E.Yu. Ageev. FTT **43**, *2*, 242 (2001) (in Russian).
[9] E.S. Khudyakova, A.N. Grebenchukov, M.G. Kisteneva, Yu.F. Kargin. Elektronika, izmeritel'naya tekhnika, radiotekhnika i svyaz. Dokladi TUSURa **2**, *26*, 63 (2012) (in Russian).

[10] R.A. astro-Arata, G.I. Grabko, A.A. Kononov, N.I. Anisimova, M. Krbal, A.V. Kolobov. FTP **55**, *5*, 450, (2021) (in Russian).
[11] R.A. Kastro, N.I. Anisimova, A.A. Kononov. FTP **52**, *8*, 912 (2018) .
[12] A.V. Ilyinsky, V.M. Kapralova, R.A. Castro, L.A. Nabiullina, V.M. Stozharov, E.B. Shadrin. FTT **60**, *9*, 1785 (2018) (in Russian).
[13] B. Briat, V.G. Grachev, G.I. Malovichko, O.F. Schirmer, M. Wöhlecke. In: *Defects in Inorganic Photorefractive Materials and Their Investigations* / P. Gnter, J.-P.Huignard eds. Springer Series in Optical Sciences. V. 114, Springer, N.Y. (2007). P. 9–49.
[14] O.F. Schirmer, H.J. Reyher, M Wöhlecke. In: Insulating Materials for Optoelectronics / F. Agullo-Lopez, ed. World Scientific, Singapore (1995). V. 3. P. 93.
[15] L. Wiehl1, A. Friedrich, E. Haussuh, W. Morgenroth, A. Grzechnik, K. Friese, B. Winkler, K. Refson, V. Milman. J. Phys. Condens. Matter **22**, 505401 (2010).
[16] G.L. Miessler, P.J. Fischer, D.A. Tarr. Inorganic Chemistry. 5th ed. Pearson Education, Boston (2013). 672 p.
[17] D.S. Vavilapalli, A.A. Melvin, F. Bellarmine, R. Mannam, S. Velaga, H.K. Poswal, A. Dixit, M.S. Ramachandra, R.S. Sing. Scientific Reports **10**, 22052 (2020).
[18] W. Shan, W. Walukiewicz, J.W. Ager, E.E. Haller, J.F. Geisz. Phys. Rev. Lett. **82**, *6*, 1221 (1999).
[19] L.T. Bugaenko, S.M. Ryabykh, A.L. Bugaenko. Vestn. Mosk. Univ. **49**, *6*, 363 (2008).
[20] I. Gorczyca, A. Kamińska, G. Staszczak, R. Czernecki, S.P. Łepkowski, T. Suski, H.P.D. Schenk, M. Glauser, R. Butté, J.-F. Carlin, E. Feltin, N. Grandjean, N.E. Christensen, A. Svane. Phys. Rev. B **81**, 235206 (2010).
[21] P.P. Kiran. Asian J. Phys. **30**, *6*, 917 (2021).
[22] B. Kostova, L. Konstantinov. J. Phys. Conf. Ser. **253**, 012029 (2010).
[23] A.V. Il'insky. Avtoref. dokt. diss. FTI im. A.F. Ioffe. SPb (1992) (in Russian).
[24] Khimicheskaya entsiklopediya v 5 tomakh. / Pod red. I.L. Knunyants. Nauka, M. (1990). V. 2 (in Russian).
[25] N.K. Morozova, D.A. Mideros, N.D. Danilevich. *Oxygen in Optic of Compounds II–VI of View of Theory Anticrossing Zones*. LAP, Saarbrucken (2013). 205 p. [in Russian].
[26] J. Wu, W. Walukiewicz, E.E. Haller. Phys. Rev. B **65**, 233210 (2002).
[27] G. Ouyang, C.Q. Sun, W.G. Zhu. J. Phys. Chem. C. **113**, 9516 (2009).
[28] S.H. Wei, A. Zunger. Phys. Rev. B, **60**, *8*, (1999).
[29] T.V. Panchenko, K.Yu. Strelets. FTT **51**, *2* 277 (2009) (in Russian).
[30] T. Toyoda, H. Nakanishi, S. Endo, T. Irie. J. Appl. Phys. **61**, *1*, 2065 (1987).

Translated by A.Akhtyamov